J. Min. Metall. Sect. B-Metall. 61 (2) (2025) 269 - 281

Journal of Mining and Metallurgy, Section B: Metallurgy

OPTIMIZING CALCIUM ADDITIONS FOR A STRENGTH–CORROSION RESISTANCE BALANCE IN SQUEEZE-CAST Zn–Al–Cu–Mg ALLOYS

T. Gopalakrishnan *, S.R. Sankaranarayanan, S.P.K. Babu

Department of Metallurgical and Materials Engineering, National Institute of Technology, Tiruchirappalli, India

(Received 15 June 2025; Accepted 10 October 2025)

Abstract

In this study, squeeze-cast Zn–Al–Cu–Mg alloys with varying Ca additions (0, 0.5, 1.0, and 1.5 wt.%) were investigated to evaluate the combined effects of microstructural evolution on mechanical and corrosion performance. Microstructural analysis showed a transition from coarse Zn-rich dendrites in the base alloy to a refined and uniform morphology with Ca additions up to 1.0 wt.%, followed by coarsening and increased porosity at 1.5 wt.% Ca due to excessive intermetallic formation. Mechanical testing indicated that the alloy with 1.0 wt.% Ca had the highest hardness (141 HV0.1) and tensile strength (359 MPa), attributed to grain refinement and dispersion strengthening, though with reduced ductility due to intermetallic brittleness. Electrochemical corrosion tests in 3.5 wt.% NaCl solution showed that the corrosion rate decreased from the base alloy to 1.0 wt.% Ca, confirming enhanced corrosion resistance due to microstructural refinement and protective film formation. However, excessive Ca addition (1.5 wt.%) increased the corrosion rate to 0.8109 mpy due to coarse intermetallics and porosity, which promoted localized attack. The results highlight that optimal Ca addition (1.0 wt.%) achieves a balance between strength, hardness, and corrosion resistance, making Ca-modified Zn–Al–Cu–Mg alloys promising candidates for structural and functional applications.

Keywords: *Squeeze casting; Zinc- aluminium alloy; Mechanical properties; Corrosion resistance*

1. Introduction

Zinc-based casting alloys (notably Zn–Al systems) are of growing interest for lightweight structural and tribological components because they combine good castability with moderate mechanical strength and intrinsic corrosion resistance [1]. However, their corrosion performance is susceptible to microstructural features such as dendrite morphology, grain size, and the presence and distribution of intermetallic phases. In chloride-bearing environments, micro-galvanic coupling between Zn-rich matrix regions and Al or Cu-rich intermetallics often controls the onset and propagation of localized attack, making alloy chemistry and solidification control critical design variables for improving durability [2]. Recent microstructural-corrosion studies of zinc and zinc-alloy systems emphasize that microalloying and controlled phase morphology can shift corrosion kinetics substantially, motivating targeted alloy design to balance mechanical and environmental performance [3–5].

Calcium (Ca) has emerged as a practical micro-alloying addition in various light-metal systems because of its strong influence on nucleation behavior and intermetallic formation [6]. In Zn-based alloys, Ca readily combines with Zn and Al to form Ca-rich intermetallics (e.g., Ca_1Zn_{13}, Al_2Ca_1Zn) that nucleate early during solidification and modify the eutectic/eutectoid reaction pathways; this often produces grain refinement and more homogeneous microstructures at moderate additions [7–9]. Such refinement can adequately reduce the size and number of micro-galvanic cells, improving corrosion film formation and adherence and lowering anodic dissolution rates in many environments. Experimental studies on Zn–Ca–Cu and related systems have reported that limited Ca additions can improve uniform corrosion resistance by refining grain structure and stabilizing surface films [10, 11].

Nevertheless, the electrochemical role of Ca-rich intermetallics is complex and condition-dependent. Several investigations have shown that some Ca-containing phases (notably Ca_1Zn_{13}) are cathodic relative to the Zn matrix and can accelerate localized corrosion through micro-galvanic action when coarse, continuous, or clustered [12–14]. In-situ SEM and time-lapse work have demonstrated preferential

Corresponding author: thiyages10@gmail.com

https://doi.org/10.2298/JMMB250615021G

corrosion of Ca-rich intermetallics with consequent local alkalization and ion release that can, paradoxically, either promote protective deposits or amplify pitting depending on the electrolyte and phase morphology [15, 16]. Thus, while moderate Ca additions often produce beneficial grain refinement and improved bulk corrosion metrics, excessive Ca tends to produce coarse cathodic particles and increased porosity, which are commonly associated with elevated localized corrosion rates. The trade-off between the advantages of refining and the galvanic degradation caused by intermetallics remains demonstrated in recent Zn and Mg-based alloys investigations [17–19].

Recent investigations have confirmed that small additions of calcium can markedly influence the corrosion behavior of light-metal alloys. For instance, T. Mandal et al. reported that Ca-modified Mg–Al–Zn–Sr alloys exhibited improved corrosion resistance due to grain refinement and the formation of protective surface layers. However, excessive Ca promoted coarse intermetallics and localized attack [20]. Similarly, a study on High-Zn containing Al–Zn–Mg–Cu alloys highlighted that microstructural refinement and controlled intermetallic precipitation suppressed corrosion currents and delayed pit initiation [21]. In Zn–Al–Mg systems, adding minor alloying elements also reduced corrosion rates by stabilizing corrosion films and minimizing micro-galvanic effects [22]. Zhang et al. noted similar trade-offs in Mg-Zn-Ca systems, where $Ca_2Mg_6Zn_3$ phases improved corrosion and strength but compromised elongation [23]. Doroshenko et al. studied Al-6%Mg-2%Ca-2%Zn alloys and linked phase formation to casting parameters and mechanical response [24]. These findings are consistent with our results, where moderate Ca additions (~1.0 wt.%) reduced corrosion rate, while higher levels (1.5 wt.%) deteriorated performance due to coarse $CaZn_{13}$ intermetallics and porosity. The novelty of systematically examining Ca's role in squeeze-cast Zn–Al–Cu–Mg alloys is reinforced by situating our results within these recent studies.

Given these competing effects, there is a clear need for systematic studies that correlate Ca concentration, intermetallic morphology, porosity, mechanical strength, and electrochemical behavior under the same processing route. Squeeze casting, which applies pressure during solidification, can further affect porosity, phase distribution, and film layer formation. Therefore, assessing Ca's influence specifically in squeeze-cast Zn–Al–Cu–Mg alloys is significant for engineering applications. Thus, the present work investigates Ca additions from 0 to 1.5 wt.% under identical squeeze-casting conditions and evaluates microstructure (via SEM/EDS, XRD), mechanical (tensile strength, hardness), and electrochemical corrosion performance. This combined approach allows us to identify the Ca concentration range that optimizes both mechanical performance and corrosion resistance, and to explain the underlying mechanisms in terms of intermetallic chemistry and morphology.

2. Materials and methods

2.1. Alloy Preparation

The schematic diagram of the squeeze casting setup used in the present study is shown in Figure 1. A commercial grade Zn-Al alloy consisting of 94.95 wt.% Zn, 4.0 wt.% Al, 1.0 wt.% Cu, and 0.05 wt.% Mg were used as the base alloy. Base Alloy with pure metallic calcium was added in varying amounts (0.5 wt.%, 1.0 wt.%, and 1.5 wt.%) to produce Ca-reinforced Zn-Al-Cu-Mg alloys. The Zn-Al-Cu-Mg alloy ingot was sectioned into four equal parts using an abrasive cutting machine, then weighed according to the required composition. The alloy pieces were subsequently placed in a graphite-coated crucible (10 kg capacity) inside the electric furnace for melting.

The Zn–Al–Cu–Mg alloys were prepared by melting the base metals, followed by the precise addition of pure metallic calcium to achieve the target compositions. The mixture was homogenized using a stir motor to ensure uniform distribution of elements. Before casting, the graphite-coated crucible and the cast-iron mold were preheated to 180–215 °C. Melting was done in a graphite-coated crucible using an electric bottom-pour furnace under an inert argon atmosphere at 600 ± 10 °C. After each calcium addition, the melt was manually stirred for 1–3 minutes to promote uniformity. To minimize gas porosity and oxide inclusions, the melt was degassed with high-purity argon for 10 minutes using a rotating submerged lance, which effectively removed dissolved hydrogen and dross. Preheated reinforcement was introduced at 550 °C while stirring at 250 rpm, and Ca additions held the melt for 20 minutes with continuous stirring. The Slag was carefully skimmed off the surface before transferring the melt to a preheated cylindrical squeeze die maintained at 200 °C and squeeze cast under 90 MPa using a vertical hydraulic press, with pressure maintained for 60 s to ensure complete filling and solidification. Cooling under pressure prevented porosity and thermal cracking. The solidified billets were ejected and cooled to room temperature before being sectioned into specimens for metallurgical and mechanical characterization. For chemical composition analysis, square samples (20 × 20 × 5 mm^3) for optical emission spectroscopy (OES), and the final composition results are presented in Table 1.

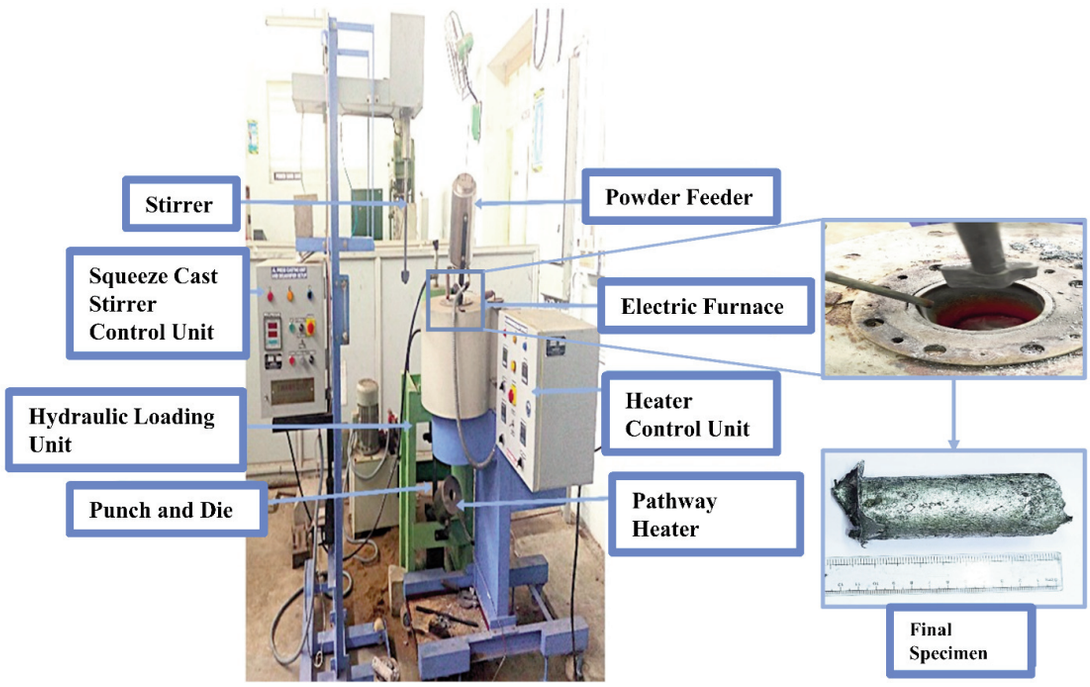

Figure 1. *Schematic representation of the squeeze casting setup*

Table 1. *Chemical Composition of Zn-Al-Cu-Mg alloy with different Ca additions (wt.%)*

Specimen	Al	Cu	Mg	Ca	Zn
Zn-Al-Cu-Mg (Base Alloy)	4	1	0.05	...	Bal.
Zn-Al-Cu-Mg + 0.5 wt.% Ca	3.66	0.96	0.0443	0.45	Bal.
Zn-Al-Cu-Mg + 1.0 wt.% Ca	3.53	0.95	0.0422	0.93	Bal.
Zn-Al-Cu-Mg + 1.5 wt.% Ca	3.49	0.93	0.0418	1.36	Bal.

2.2. Microstructural and Mechanical Characterization

The actual density of each cylindrical specimen was measured using a METTLER TOLEDO New Classic MF densitometer, based on the mass ratio to volume. The theoretical density was calculated using the rule of mixtures from the elemental compositions, and porosity was estimated by comparing the measured and theoretical densities. Samples were sectioned from the cast billets, cleaned with acetone, and prepared as square specimens (10 × 10 × 5 mm³). Each specimen was hot-mounted in resin, ground sequentially with SiC papers (240–1200 grit), and polished with 1 µm alumina slurry, followed by final buffing with 1 µm diamond paste to reveal the microstructure features. The Zn-Al-Cu-Mg alloy with varying Ca addition of (0.5 - 1.5 wt.%) Ca etched the polished surfaces with 2% Nital for 5 s and was examined using a Leica DM2500M optical microscope to evaluate grain boundary integrity and the distribution of second-phase particles. Squeeze cast specimens were further analyzed for intermetallic phases by scanning electron microscopy (SEM) coupled with energy-dispersive X-ray spectroscopy (EDS). X-ray diffraction (XRD) analysis was performed on a Pan-Analytical diffractometer using Co-Kα radiation (λ = 0.154 nm) over a 2θ range of 20°–80° at a scan rate of 2°/min. The diffraction peaks were compared with ICDD standards to identify crystalline phases. Vickers microhardness measurements were conducted per ASTM E92 using a Matsuzawa MMT-X7 tester at a 100 gf load and 15 s dwell time. Microhardness carried out five replicas of readings for each composition. Tensile testing was conducted using a Tinius Olsen H25KT micro-universal testing machine at a 0.2 mm/min crosshead speed. Sub-size specimens, machined via wire EDM in compliance with ASTM E8/E8M, had a gauge length of 6.0 mm, a width of 4 mm, and a thickness of 1.0 mm. The reported tensile strength values represent the average of three tests to ensure statistical accuracy.

2.3. Potentiodynamic Polarization Test

The corrosion behavior of the squeeze-cast Zn–Al–Cu–Mg alloys with varying Ca contents (0, 0.5, 1.0, and 1.5 wt.%) was evaluated using electrochemical methods. Potentiodynamic polarization (PDP) tests were carried out using a three-electrode cell connected to a Gill ACM electrochemical workstation, with the alloy specimen as the working electrode, platinum as the counter electrode, and saturated calomel electrode (SCE) as the reference. The samples were stabilized at open-circuit potential (OCP) for 30 min before scanning from −650 mV to +350 mV relative to OCP at a scan rate of 1 mV s^{-1}. Corrosion current density (I_{corr}) and corrosion potential (E_{corr}) values were extracted using Tafel extrapolation, and the corrosion rate was calculated using formula (a) and surface morphologies of corrosion specimens were examined using FESEM analysis.

$$CR = \frac{0.13 \cdot EW \cdot i_{corr}}{\rho \cdot A} (\text{mpy}) \quad \text{(a)}$$

Where, EW = equivalent weight (g) , icorr = corrosion current (μA), ρ = density (g/cm^3) A = exposed surface area (cm^2).

3. Results and discussion

3.1. Microstructural Evolution

The microstructures of the squeeze-cast Zn-Al-Cu-Mg alloy with varying calcium additions are shown in Figure 2. The optical images reveal a transition from coarse dendritic structures in the unreinforced alloy to a finer and more uniform morphology in the calcium-reinforced samples. The Zn-Al alloys exhibit Al and Zn-rich solid solutions whose distribution varies with calcium content, as illustrated in Figure 2a. The unreinforced alloy features coarse Zn-rich dendrites and eutectoid colonies Figure 2a. In the Zn-3.5Al-0.9Cu-0.04Mg alloy with 1.5 wt.% calcium Figure 2d, the microstructure comprises Ca_1Zn_{13} and Ca_1Mg_2 intermetallic phases, along with a newly formed Zn-Al phase [5, 25]. The $CaZn_{13}$ phase appears in dendritic or blocky forms and exhibits lower brightness than the Al_1Cu + Cu_6Zn phases, as calcium is approximately 13% lighter than aluminium. Al-Zn particles observed to attach to Ca_1Zn_{13}, forming a compound structure confirmed by XRD analysis [9]. The characteristic dendritic morphology of Ca_1Zn_{13} is shown in Figure 3—a comparison between the unreinforced and 1.5 wt.% Ca-reinforced alloys

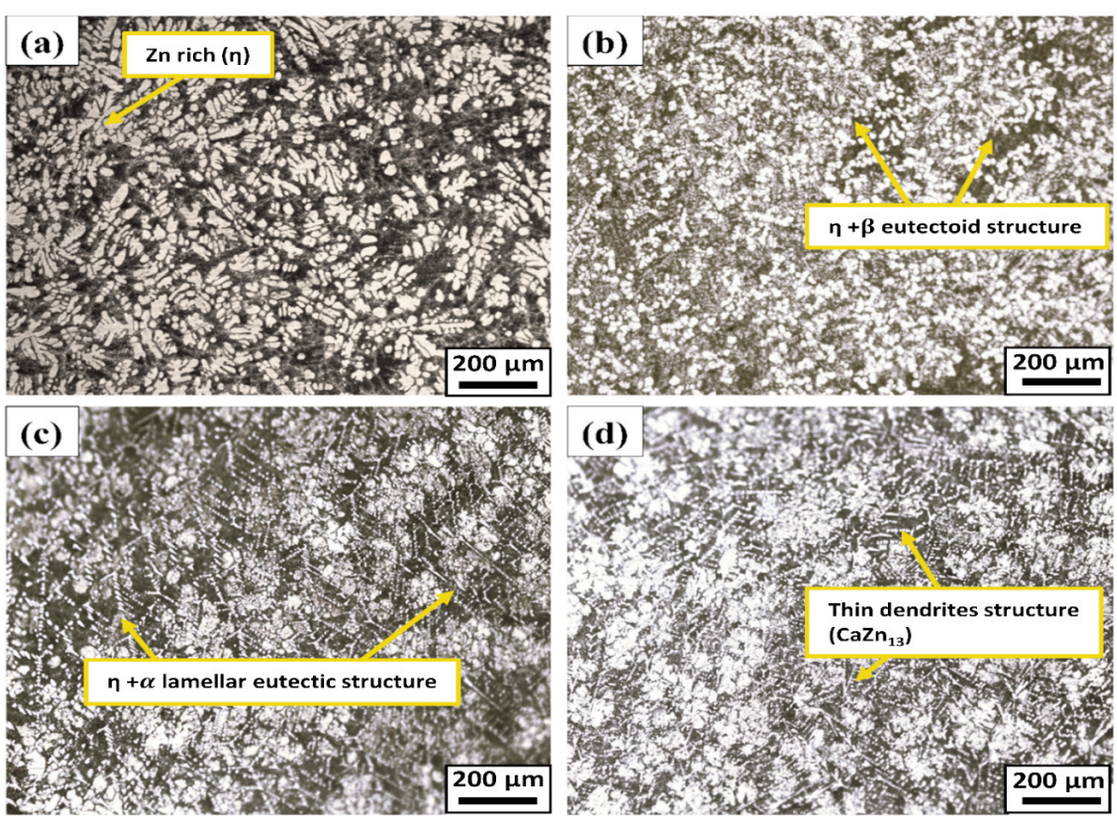

Figure 2. *Optical Micrographs of Zn-Al-Cu-Mg Alloys with different Ca additions. (a) base alloy; (b) 0.5 wt.% Ca; (c) 1.0 wt.% Ca; (d) 1.5 wt.% Ca*

Figure 2d show that calcium addition modifies the dendritic morphology. The secondary dendritic arm spacing improved, and the overall grain structure became more consistent, even though the Zn-rich dendrites appear slightly longer. This microstructural refinement is associated with enhanced mechanical properties up to an optimal calcium content.

The FESEM images and EDS analysis with mapping show the phase distribution in the mid-region of Zn-Al-Cu-Mg alloys with varying calcium contents, as shown in Figure 3. The base alloy microstructure (Figure 3a) consists of bright white globular grains, with delicate lamellar and coarse cellular structures. In the alloy containing 1.5 wt.% Ca (Figure 3d), slower cooling resulted in the formation of larger dendritic phases, lamellar eutectic structures, and darker regions at dendrite boundaries containing fine eutectoid lamellae. According to the Zn-Al phase diagram, hypoeutectic Zn-Al alloys primary solidify as α-Zn, followed by a eutectic reaction forming a mixture of α-Zn and α-Al phases upon cooling. EDS analysis in Figure 3a revealed high Zn and Al content, corresponding to the η-Zn matrix, and exhibited a similar Zn-Al composition, indicative of the AlZn phase. In Figure 3b, EDS provides further phase identification. It corresponds to the Ca_1Mg_2 phase and is in a lighter dendritic region. It shows a Zn-rich composition with minor Al and Cu, aligning with the η-Zn phase, and corresponds to a Zn-rich eutectoid region. Figure 3c shows elevated Ca and Al and traces of Mg and Cu, suggesting the presence of the Al_2Ca_1Zn phase [23, 26, 27]. EDS

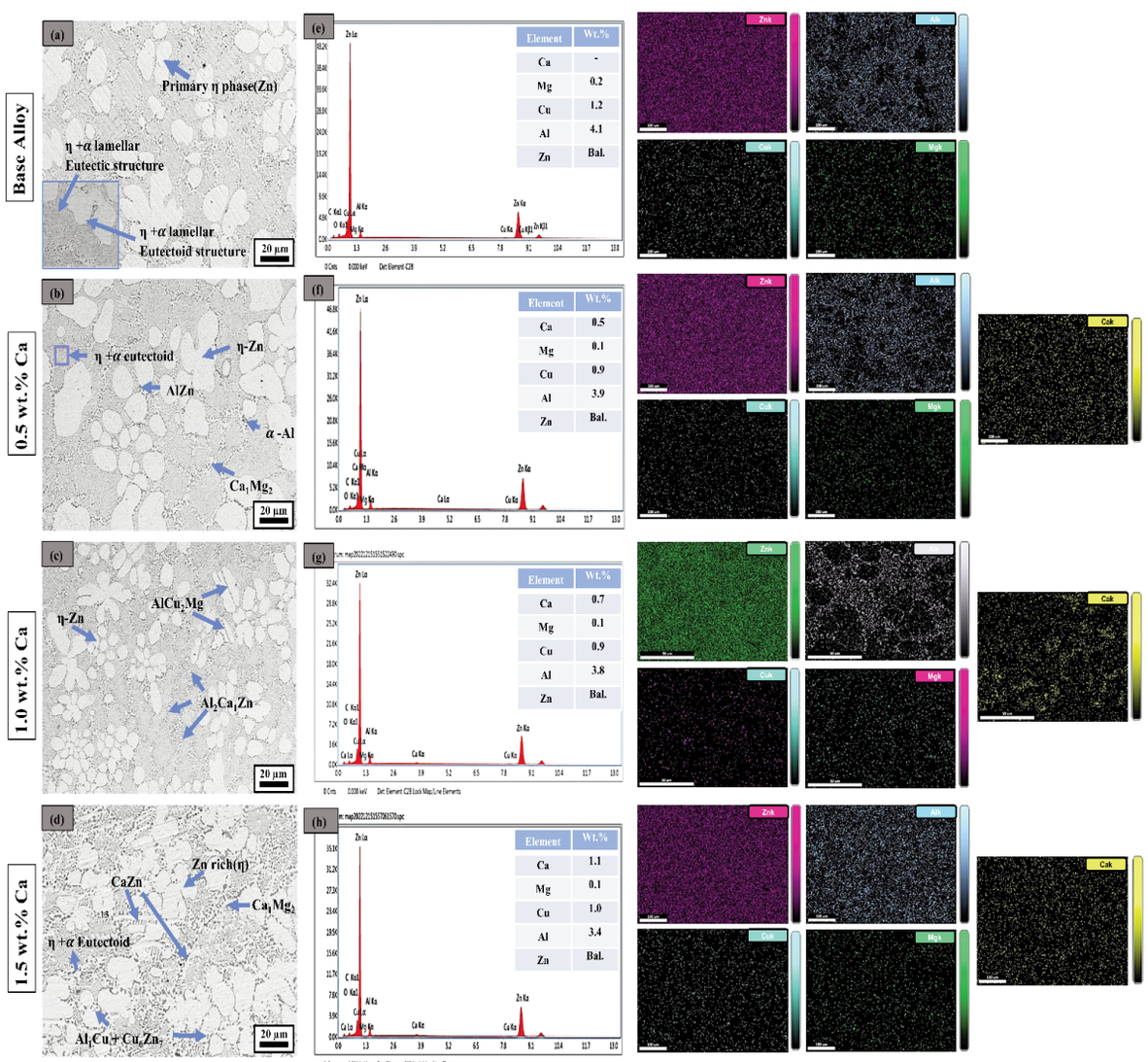

Figure 3. *(a-d) FESEM Morphology of the Zn-Al-Cu-Mg alloy without and with Ca addition, (e-h) showing EDS analysis with mapping*

analysis shows higher Al, Mg, and Cu, consistent with the $AlCu_2Mg$ phase. It reveals a Zn-rich region with Ca content matching the Ca_1Zn_{13} phase. Brighter zones are predominantly Zn-rich. Higher calcium content was also observed, with similar features at 1.5 wt.% Ca alloy (Figure 3d), where regions containing Ca, Al, and Cu likely correspond to complex phases such as Al_1Cu, Cu_6Zn_7, and Ca_1Zn_{13}. Darker areas show high Ca content, confirming the presence of Ca_1Zn_{13}; the brighter regions remain Zn-rich. Corresponding SEM morphologies and XRD peaks support these interpretations at 2θ values matching Ca_1Zn_{13}, Ca_1Mg_2, and Al_2Ca_1Zn [14] —alloys containing 0.5 wt.% and 1.0 wt.% Ca showed microstructures and phase compositions similar to the 1.5 wt.% Ca alloy. Coarse dendrites in Ca-free and Ca-containing alloys contain Ca_1Zn_{13}, while Ca_1Zn_{13} and Ca_1Mg_2 precipitates are present in the 1.0 and 1.5 wt.% Ca samples. $CaZn_{13}$ and Ca_1Mg_2 phases become more prominent at higher Ca contents (≥1.0 wt.%), as evidenced by the increased intensity of their XRD peaks. Trace amounts may also be present at 0.5 wt.% Ca but are below clear detection limits. In Figure 3d, the Ca_1Zn_{13} phase lies between the primary Zn and eutectoid Zn + Al regions. Calcium addition refined the eutectic structure by slowing the eutectic and eutectoid transformation kinetics. The finest eutectoid lamellar spacing observed at 1.0 wt.% Ca, while coarser eutectoid lamellar and larger dendrites in the 1.5 wt.% Ca alloy may result from reduced Zn and Al diffusion rates, promoting lamellar growth rather than new lamellae nucleation [28]. Although EDS alone cannot confirm phase identity, the observed compositional trends, SEM morphology, and XRD data provide robust evidence for accurate phase characterization.

3.2. XRD Result

The X-ray diffraction (XRD) patterns shown in Figure 4 demonstrate the effects of calcium additions, ranging from 0.5 wt.% to 1.5 wt.% on the base Zn-Al-Cu-Mg alloys. Prominent diffraction peaks correspond to the Zn phase, while minor peaks observed at 2θ ≈ 36°, 39°, and 71° are associated with the Ca_1Zn_{13}, Al_2Ca_1Zn, and Ca_1Mg_2 phases, respectively. Although these peaks are relatively weak and may overlap with those of Zn, the presence of the intermetallic compounds was confirmed using standard ICDD reference data and corroborated through complementary EDS analysis, minimizing the risk of misinterpretation due to peak overlap. The observed variation in average grain size with increasing calcium content indicates effective grain refinement in the base alloy, with reinforcement occurring progressively up to 1.5 wt.% Ca.

With increasing calcium content, additional peaks gradually emerge, which remain challenging when forming intermetallic compounds such as Ca_1Zn_{13} and Al_2Ca_1Zn. However, due to overlapping peak positions with Zn-rich phases, the reliable identification of these minor phases using XRD alone remains challenging. Calcium addition appears to promote grain refinement through two primary mechanisms: (1) the suppression of grain growth during solidification via the formation of Zn-Ca precipitates, particularly the dendritic Ca_1Zn_{13} phase, and (2) the development of Zn-Al-based

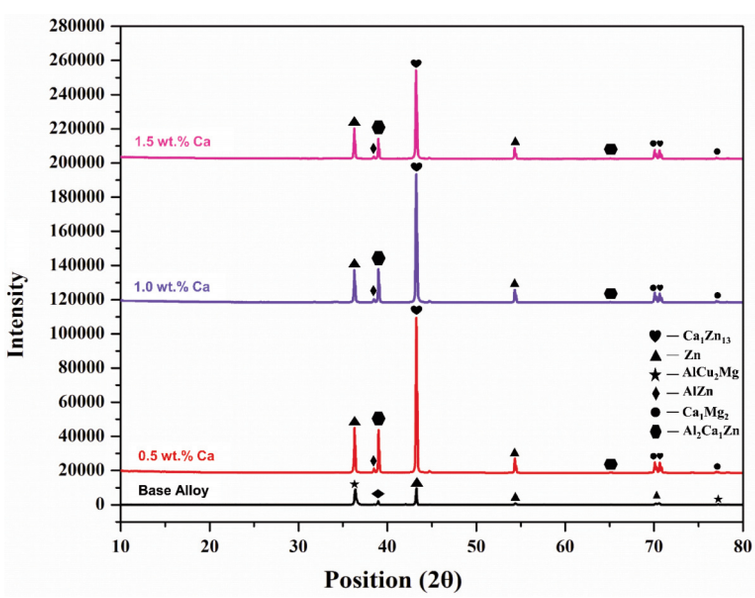

Figure 4. *XRD Patterns of squeeze cast Zn-Al-Cu-Mg Alloy with various wt.% of Ca*

intermetallics such as Al_2Ca_1Zn and $AlCu_2Mg$. These phases inhibit the formation of lamellar Zn-Ca and granular $ZnCa_1Al$ phases, contributing to enhanced mechanical strength in the squeeze-cast alloy [14]. However, calcium additions exceeding 1.5 wt.% lead to consumption of Al atoms in Zn-Ca precipitates. Ca reduces formation of the Zn-Al phases and consequently diminishes the grain-refining effect in the base alloy. The observed effect of the key phases identified by XRD and their associated impacts are summarized in Table 3.

3.3. Mechanical Properties

The microhardness values of the base Zn-Al-Cu-Mg alloy, both unreinforced and reinforced with 0.5 wt.%, 1.0 wt.%, and 1.5 wt.% Ca, are presented in Figure 5. The base alloy exhibited a microhardness of 113 HV0.1. Upon the addition of 0.5 wt.% Ca, a slight increase to 122 HV0.1 was observed, attributed to the dispersion of complex intermetallic compounds within the zinc matrix. The most significant enhancement was noted at 1.0 wt.% Ca, where microhardness increased to 141 HV0.1, indicating improved interfacial bonding and uniform distribution of Ca-containing phases within the matrix [26, 29]. At 1.5 wt.% Ca, the microhardness decreased slightly to 130 HV0.1, likely due to the formation of coarse or brittle intermetallics and increased porosity. Tensile strength of the base alloy and varying calcium additions is illustrated in Figure 5. The base alloy recorded the lowest tensile strength at 287 MPa, while the base alloy with 1.0 wt.% Ca exhibited the highest value at 359 MPa. Grain refinement and dispersion strengthening from fine intermetallic phases like Ca_1Zn_{13} and $AlCu_2Mg$ are responsible for this increase; the 0.5 wt.% Ca alloy shows a significant impact. Improvement, whereas the strength marginally decreased at 1.5 wt.% Ca due to structural coarsening and porosity. Elongation data further highlight the trade-off between strength and ductility. The base alloy elongated 9.37%, which increased to 15.6% at 0.5 wt.% Ca—indicating enhanced ductility due to refined microstructure and improved feeding. However, elongation dropped sharply at 1.0 wt.% Ca and remained low at 1.5 wt.% Ca, with the minimum

Table 2. *Key phases identified by XRD and their associated effects*

Phase	Peak Position (2θ)	d-spacing (Å)	Compound Type	Observed effect
Zn	~36°	2.5	Matrix	Base alloy structure
Ca_1Zn_{13}	~43°	2.1	Intermetallic	Strength enhancement
Al_2Ca_1Zn	~39°	2.3	Intermetallic	Brittle behavior
$AlCu_2Mg$	~36-37°	2.4-2.5	Intermetallic	Strengthening; Cu/Mg segregation
AlZn	~38°	2.3	Solid solution	Improved corrosion resistance
Ca_1Mg_2	~74°	1.28	Intermetallic	Microstructural modification

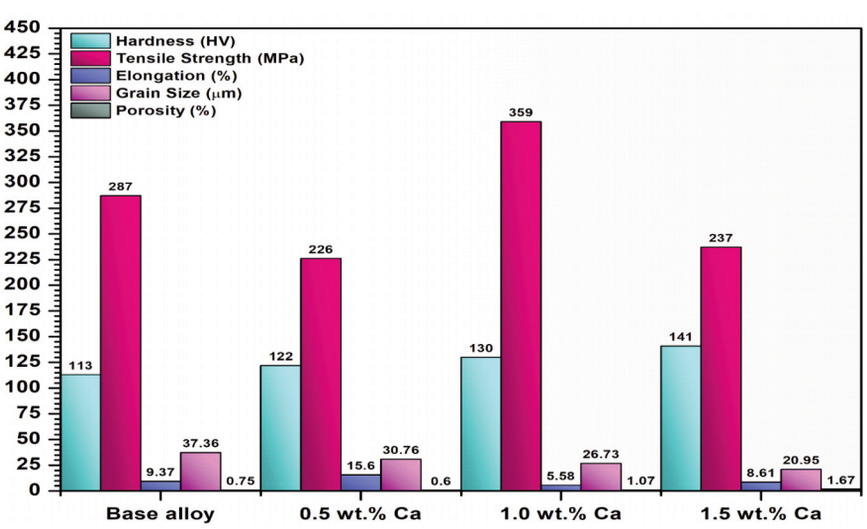

Figure 5. *Comparison of density, porosity, grain size, hardness, tensile strength, and elongation for Zn-Al-Cu-Mg alloys with different Ca additions*

observed at 1.0 wt.% Ca. Microstructural refinement and hard, brittle intermetallics that prevent dislocation motion and encourage fracture initiation are responsible for this decrease in ductility. While 1.0 wt.% Ca addition optimizes strength due to grain refinement and fine intermetallic dispersion, resulting in the lowest ductility. Ductility doesn't decrease linearly with calcium content and is affected by a complex interaction of microstructural factors. At higher Ca contents, coarse or agglomerated intermetallics may be stress concentrators, increasing crack susceptibility under tensile load.

The mechanical properties show a non-monotonic dependence on Ca content: the 0.5 wt.% Ca alloy displays slightly reduced ultimate tensile strength (UTS) but increased elongation relative to the base alloy, whereas the 1.0 wt.% Ca alloy exhibits the highest UTS, hardness, and 1.5 wt.% Ca alloy loses strength and ductility. The mechanical properties can explain the above phenomenon by considering three competing microstructural influences. First, small Ca additions (≤0.5 wt.%) promote grain refinement and improved feeding during solidification, which tends to increase ductility and reduce stress concentrations; however, at this low concentration, the volume fraction and dispersion of strengthening intermetallics are insufficient to provide substantial dispersion strengthening, explaining the modest or reduced UTS at 0.5 wt.%. Second, at an optimal addition (1.0 wt.% Ca), the alloy shows the finest eutectoid lamellae and a uniform distribution of fine Ca and Al-containing intermetallics (e.g., Ca_1Zn_{13}, Al_2Ca_1Zn, $AlCu_2Mg$), which together produce combined grain-refinement strengthening and dispersion strengthening — this yields the peak UTS and hardness. Third, at higher Ca (1.5 wt.%), excessive Ca promotes the nucleation and growth of coarse, brittle Ca-rich intermetallics, increases micro-porosity and particle agglomeration, and reduces matrix continuity; these features act as stress concentrators and crack initiation sites, reducing effective load transfer and causing the observed drop in UTS and ductility. These interpretations are supported by the micrographs (Figure 2 & Figure 3), EDS/XRD phase identification, porosity/density measurements (Table 3), and fracture surface morphologies (Figure 6), which show coarser intermetallics and increased interdendritic porosity at 1.5 wt% % Ca. Thus, the mechanical response follows a balance between beneficial grain/intermetallic refinement (strengthening) and detrimental porosity/coarsening (embrittlement), which explains the apparent inconsistencies across Ca levels.

3.4. Fractography Analysis

The fracture surfaces of the tensile specimens from the base and Ca-reinforced alloys are shown in Figure 6, illustrating the influence of calcium content on fracture behavior. The base alloy (Figure 6a) exhibits cleavage planes and river patterns characteristic of brittle fracture and mild tearing along the facets, at 0.5 wt.% Ca (Figure 6b), the fracture surface reveals the development of voids and a predominantly brittle morphology, though limited ductile dimples are present [12, 20]. Interestingly, despite its predominantly brittle features, this alloy exhibited the highest elongation among the tested compositions. This apparent inconsistency suggests that fracture morphology is not governed solely by bulk ductility but also by localized factors such as intermetallic distribution, porosity, and crack propagation paths. At 1.0 wt.% Ca (Figure 6c), the fracture surface presents a transitional mode, with a mixture of shallow dimples and faceted cleavage planes, indicating partial ductile behavior. However, coarse Ca-rich intermetallics restricted plastic deformation, reducing elongation despite the grain refinement observed in this alloy, for the 1.5 wt.% Ca alloy (Figure 6d), the fracture surface is dominated by cleavage features, intergranular cracking, and sparse dimples, reflecting a shift toward predominantly brittle failure. Although dimple-like features appear more numerous in this sample, they are generally shallow and non-uniform, often nucleated at coarse Ca_1Zn_{13} intermetallics or interdendritic pores. These dimples represent premature void nucleation rather

Table 3. *Physical and mechanical property evaluation of squeeze-cast Zn-Al-Cu-Mg alloys with different Ca contents*

Specimen	Theoretical Density (g/cm^3)	Measured Density (g/cm^3)	Porosity (%)	Grain size (μm)	Hardness (HV)	Tensile Strength (MPa)	Elongation (%)
Zn-Al-Cu-Mg (Base Alloy)	6.7	6.65	0.75	37.36	113	287	9.37
Zn-Al-Cu-Mg + 0.5 wt.% Ca	6.66	6.62	0.6	30.76	122	226	15.6
Zn-Al-Cu-Mg + 1.0 wt.% Ca	6.61	6.54	1.07	26.73	141	359	5.58
Zn-Al-Cu-Mg + 1.5 wt.% Ca	6.59	6.48	1.67	20.95	130	237	8.61

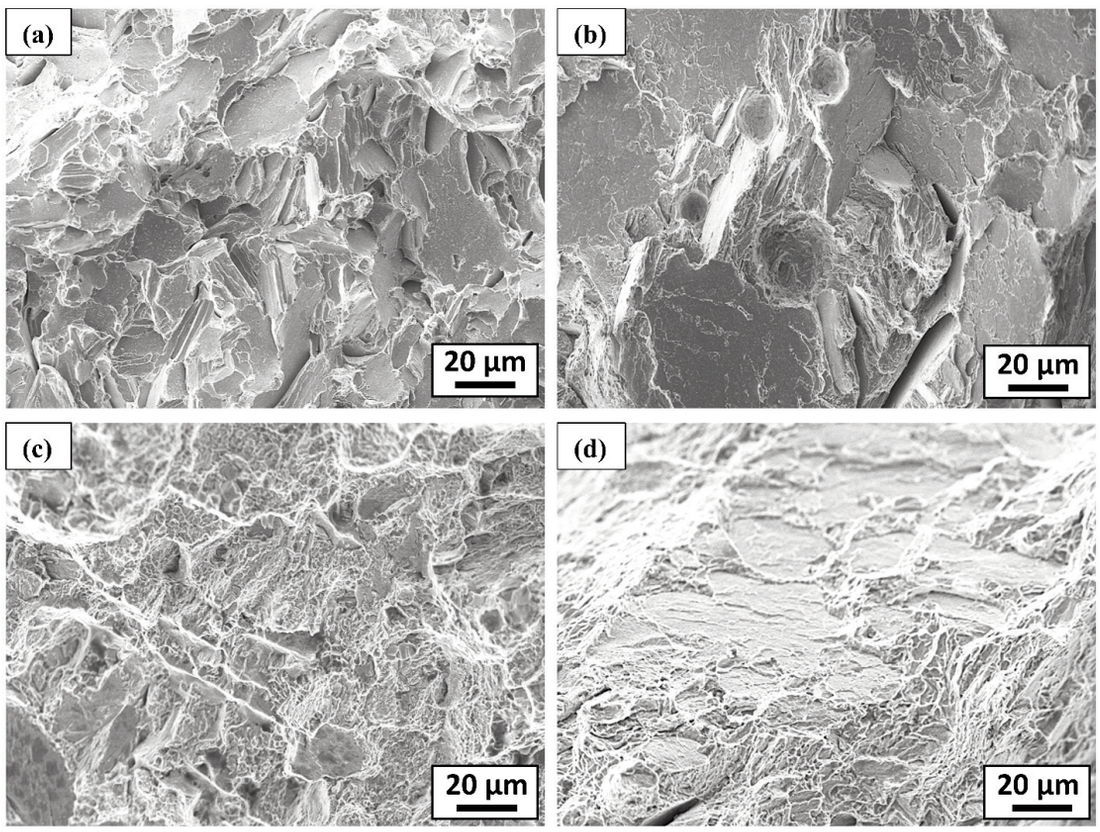

Figure 6. *SEM fracture micrographs of Zn-Al-Cu-Mg Alloys with different Ca addition (a) base alloy; (b) 0.5 wt.% Ca; (c) 1.0 wt.% Ca; (d) 1.5 wt.% Ca*

than extensive plastic tearing, explaining why the alloy exhibits the lowest elongation despite a seemingly dimpled fracture surface [11, 28].

The fracture analysis confirms that mechanical performance correlates significantly with microstructural evolution: grain refinement and uniformly dispersed intermetallics at 1.0 wt.% Ca enhances strength, whereas excessive Ca promotes porosity and coarse intermetallic formation, which act as stress concentrators and limit ductility. These findings underscore the importance of controlling intermetallic morphology and achieving uniform phase distributions to balance strength and fracture resistance in Zn–Al–based alloys.

3.5. Corrosion Behavior

The corrosion rates obtained from electrochemical measurements are summarized in Table 4. All measured corrosion rates were within the range of 0.4686 to 0.8109 mpy, indicating that the alloys exhibit moderate corrosion resistance in 3.5 wt.% NaCl, as shown in the Figure 7. A substantial correlation with calcium content was observed. The base alloy exhibited a relatively higher corrosion rate of 0.7469 mpy, attributed to coarse Zn-rich dendrites and eutectoid colonies — the addition of 0.5 wt.% Ca slightly reduced the corrosion rate to 0.7087 mpy, suggesting that limited Ca additions promote grain refinement and homogenization of the matrix, thereby mitigating galvanic interactions between Zn-rich and Al-rich regions, at 1.0 wt.% Ca, the alloys exhibited the lowest corrosion rate**,** as confirmed by PDP tests. The corrosion rate reduced to 0.4686 mpy, resulting in a 37% reduction compared to the base alloy. The enhanced microscopic structure and formation of fine Ca-rich intermetallics (Ca_1Zn_{13} and Al_2Ca_1Zn) contributed to this performance improvement. They probably contributed to developing a more protective surface film and reduced the risk of localized corrosion. However, at higher Ca content (1.5 wt.%), the corrosion rate increased sharply to 0.8109 mpy, exceeding the base alloy's. FESEM micrographs (Figure 8b) revealed localized pitting and intergranular corrosion in regions enriched with coarse Ca-rich intermetallics. Combined with the higher porosity at this composition, these phases likely acted as preferential corrosion sites and accelerated localized attack.

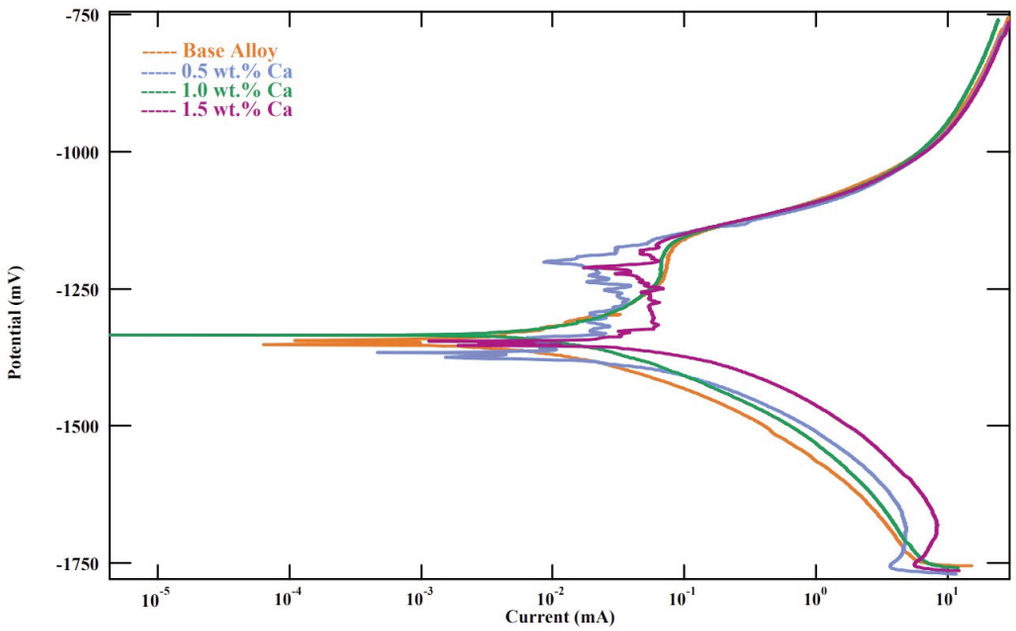

Figure 7. *Potentiodynamic polarization curves of Zn–Al–Cu–Mg alloys with varying Ca contents (0–1.5 wt.%) in 3.5 wt.% NaCl solution*

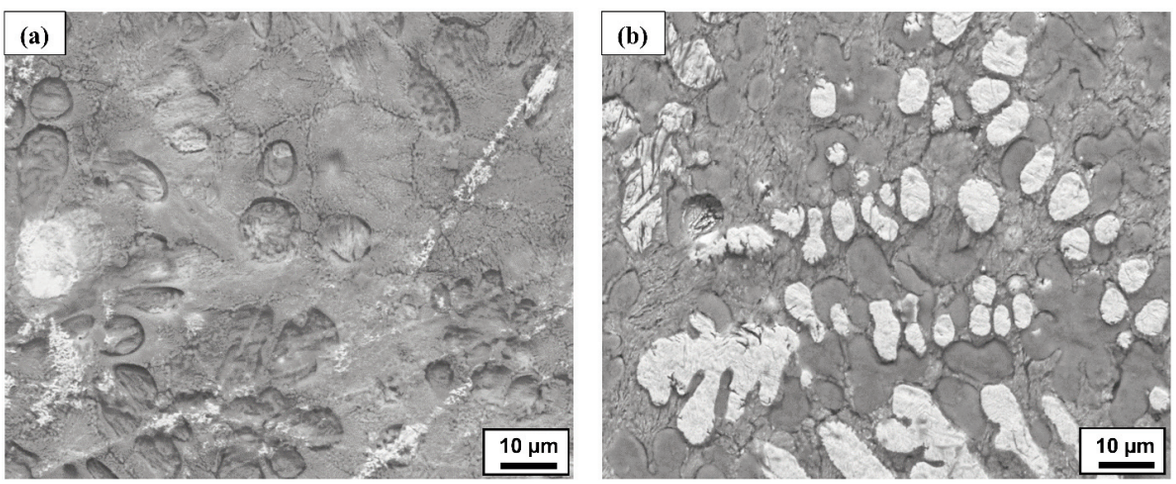

Figure 8. *FESEM micrographs of corroded surface (a) base alloy and (b) 1.0 wt.% Ca*

Table 4. *Potentiodynamic polarization results of Zn–Al–Cu–Mg alloys with varying Ca contents*

Specimen	$E_{corr\ (mV)}$	I_{corr} (µA/cm²)	Corrosion Rate (mpy)
Zn-Al-Cu-Mg (Base Alloy)	-1344.8	0.5986205	0.74687
Zn-Al-Cu-Mg + 0.5 wt.% Ca	-1365.9	0.57253	0.7087
Zn-Al-Cu-Mg + 1.0 wt.% Ca	-1343.4	0.3708541	0.4686
Zn-Al-Cu-Mg + 1.5 wt.% Ca	-1342.7	0.6306576	0.8109

Overall, the results demonstrate that moderate Ca addition (≈1.0 wt.%) enhances the corrosion resistance of Zn–Al–Cu–Mg alloys by promoting microstructural refinement and stable intermetallic distributions. In contrast, excessive Ca addition (≥1.5 wt.%) deteriorates corrosion performance due to the precipitation of coarse, electrochemically heterogeneous intermetallics and increased porosity.

4. Conclusion

The present study investigated the effects of calcium (Ca) reinforcement on the microstructure mechanical properties, and corrosion resistance of

squeeze-cast Zn-Al-Cu-Mg alloys. The findings led to the following conclusions:

• Microstructural evaluation revealed that moderate Ca additions, particularly at 1.0 wt.%, contributed to grain refinement and facilitated the formation of intermetallic phases such as Ca_1Zn_{13} and Al_2Ca_1Zn. These microstructural modifications resulted in an enhancement of tensile strength and hardness. However, further increases in Ca content beyond 1.0 wt.% resulted in the coarsening of intermetallic compounds and an uneven distribution, adversely affecting ductility and structural homogeneity.

• X-ray diffraction (XRD) patterns confirmed the presence of Zn as the primary matrix phase, while Ca_1Zn_{13} and Al_2Ca_1Zn emerged as dominant secondary phases. Their influence on the alloy's properties varied with their morphology and distribution, strengthening the alloy at moderate levels but contributing to brittleness when present in excessive amounts.

• Mechanical testing confirmed that the alloy containing 1.0 wt.% Ca achieved the optimal combination of high tensile strength and moderate ductility, reflecting a well-balanced microstructure. Fracture surface analysis via SEM showed a transition from mixed ductile-brittle fracture modes at lower Ca content (0.5–1.0 wt.%) to predominantly brittle cleavage and intergranular cracking at higher Ca contents (1.5 wt.%). The fracture mechanisms were strongly affected by the size and distribution of Ca-rich intermetallics, as well as porosity and localized stress concentration effects. High-magnification insets of fracture surfaces revealed characteristics such as micro void coalescence and cleavage planes, providing deep insights into the failure mechanisms influenced by calcium concentration.

• Potentiodynamic polarization results demonstrated that the addition of 1.0 wt.% Ca provides the best corrosion resistance, with the lowest corrosion current density and most stable passive film. Higher Ca content (1.5 wt.%) resulted in degradation of corrosion resistance due to intermetallic coarsening and potential galvanic effects.

• Future studies should focus on the wear performance, thermal stability, and fatigue resistance of Ca-reinforced Zn-Al-Cu-Mg alloys to expand upon this work.

Acknowledgments

The authors thank the Corrosion & Surface Engineering Laboratory, Department of Metallurgical and Materials Engineering, NIT Trichy, for providing the necessary facilities to conduct the present investigation.

Author Contributions

Thiyagesan G - Material preparation, Data collection, Formal analysis, Writing- original draft. Sankara Raman Sankaranarayanan - Responsible mentor & Supervision, Writing - review & editing. S.P. Kumaresh Babu - Experimental resources, Writing - review & editing, Supervision & Visualization.

Data availability statement

Data will be made available on request.

Conflict of Interest

The corresponding author, representing all authors, declares no conflict of interest.

References

[1] Z. Wu, S. Sandlöbes, L. Wu, W. Hu, G. Gottstein, S. Korte-Kerzel, Mechanical behaviour of Zn–Al–Cu–Mg alloys: Deformation mechanisms of as-cast microstructures, Materials Science and Engineering: A, 651 (2016) 675–687. https://doi.org/10.1016/j.msea.2015.11.020

[2] H. Zhou, J. Wei, G. Tian, R. Qie, L. Yan, A. Zhao, Effect of al content on microstructure and corrosion resistance of Zn-Al-Mg alloy, Materials Science and Technology, (2024). https://doi.org/10.1177/02670836241292174

[3] L. Jiang, Z. Zhang, Y. Bai, Y. Wang, W. Mao, Design of novel Al-Mg-(Zn-Sc) alloys with enhanced mechanical properties and corrosion resistance, Journal of Alloys and Compounds, 969 (2023) 172425. https://doi.org/10.1016/j.jallcom.2023.172425

[4] D. Pradhan, A. Mondal, A. Chakraborty, M. Manna, M. Dutta, Microstructural investigation and corrosion behavior of hot-dipped Al-Si-Mg-Cu alloy coated steel, Surface and Coatings Technology, 375 (2019) 427–441. https://doi.org/10.1016/j.surfcoat.2019.07.047

[5] A. Pola, M. Tocci, F.E. Goodwin, Review of microstructures and properties of zinc alloys, Metals, 10 (2020) 253. https://doi.org/10.3390/met10020253

[6] T. Fu, L. Ma, K. Lu, G. Wang, H. Shen, T. Guan, Composition design and performance analysis of Zn–0.4Mg–nCa biodegradable alloys, Journal of Materials Research, 39 (2024) 2589–2600. https://doi.org/10.1557/s43578-024-01409-2

[7] Y. Zhang, G. Wu, W. Liu, L. Zhang, S. Pang, Y. Wang, W. Ding, Effects of processing parameters and Ca content on microstructure and mechanical properties of squeeze casting AZ91–Ca alloys, Materials Science and Engineering: A, 595 (2014) 109–117. https://doi.org/10.1016/j.msea.2013.12.014

[8] J. Li, L. Chang, B. Chen, H. Huang, Z. Guo, Effects of processing technology on the electrochemical behavior and Zn deposition process of Al-Mn-Ca alloy cathodes

in high Cl− ions $ZnSO_4$ solutions, Journal of Solid State Electrochemistry, 26 (2022) 2527–2539. https://doi.org/10.1007/s10008-022-05272-1

[9] M. Luqman, Y. Ali, M.M.Y. Zaghloul, F.A. Sheikh, V. Chan, A. Abdal-hay, Grain refinement mechanism and its effect on mechanical properties and biodegradation behaviors of Zn alloys – A review, Journal of Materials Research and Technology, 24 (2023) 7338–7365. https://doi.org/10.1016/j.jmrt.2023.04.219

[10] D. Wang, J. Zhang, J. Xu, Z. Zhao, W. Cheng, C. Xu, Microstructure and corrosion behavior of Mg–Zn–Y–Al alloys with long-period stacking ordered structures, Journal of Magnesium and Alloys, 2 (2014) 78–84. https://doi.org/10.1016/j.jma.2014.01.008

[11] Y. Xiao, Y. Cai, W. Yao, D. Zhuang, F. Chen, T. Li, Y. Zhong, C. Luo, W. Chen, Z. Lyu, H. Yu, Developing high elongation of Ca-containing Zn alloys with superior osteogenic and antibacterial properties, Journal of Alloys and Compounds, 1010 (2025) 176988. https://doi.org/10.1016/j.jallcom.2024.176988

[12] Z. Jia, Y. Yu, Z. Mao, S. Du, Q. Chen, X. Niu, The influence of the addition of Ca, Zn, and Zr on the corrosion properties of As-homogenized Mg-3Sn alloys, Crystals, 15 (2025) 537. https://doi.org/10.3390/cryst15060537

[13] M.I. Abdulsalam, A study of crevice corrosion susceptibility of Zn-Al alloys in a high-pH environment, Metals, 13 (2023) 1698. https://doi.org/10.3390/met13101698

[14] Z.-Z. Shi, J. Yu, X.-F. Liu, H.-J. Zhang, D.-W. Zhang, Y.-X. Yin, L.-N. Wang, Effects of Ag, Cu or Ca addition on microstructure and comprehensive properties of biodegradable Zn-0.8Mn alloy, Materials Science and Engineering: C, 99 (2019) 969–978. https://doi.org/10.1016/j.msec.2019.02.044

[15] L. Xiao, Q. Liu, J. Wang, N. Chen, J. Chen, J. Song, X. Zhang, K. Xiao, Study on corrosion mechanism of Al–Zn coatings in the simulated polluted marine atmosphere, Journal of Materials Research and Technology, 25 (2023) 6446–6458. https://doi.org/10.1016/j.jmrt.2023.07.091

[16] P.K. Rai, D. Rout, D.S. Kumar, S. Sharma, G. Balachandran, Corrosion behaviour of hot-dip Zn-Al-Mg coatings with different Al content, Anti-Corrosion Methods and Materials, 69 (2022) 29–37. https://doi.org/10.1108/ACMM-05-2021-2487

[17] Y. Ding, F. Zhang, H. Zhou, S. Cheng, K. Xu, Z. Wang, S. Xie, J. Tian, Effect of Al content on the long-term corrosion behavior of arc-sprayed ZnAl alloy coatings, Coatings, 13 (2023) 1720. https://doi.org/10.3390/coatings13101720

[18] J. Duchoslav, R. Steinberger, M. Arndt, T. Keppert, G. Luckeneder, K.H. Stellnberger, J. Hagler, G. Angeli, C.K. Riener, D. Stifter, Evolution of the surface chemistry of hot dip galvanized Zn–Mg–Al and Zn coatings on steel during short term exposure to sodium chloride containing environments, Corrosion Science, 91 (2015) 311–320. https://doi.org/10.1016/j.corsci.2014.11.033

[19] E. Ahmed, H. Henein, A. Qureshi, J. Liu, The microstructure, mechanical behaviour, and dissolvability of novel Al-Cu-Zn-Mg-based alloys, Canadian Metallurgical Quarterly, 63 (2024) 440–459. https://doi.org/10.1080/00084433.2023.2219947

[20] T. Mandal, S. Dasgupta, A. Barui, S. Kundu, Microstructure, corrosion, and biological responses of Mg-Al-Zn-Sr-xCa alloys for bioresorbable applications, JOM, 75 (2023) 2299–2313. https://doi.org/10.1007/s11837-022-05595-4

[21] M. Long, F. Jiang, F. Wu, M. Wu, Y. Su, Effect of pre-strain on microstructure and corrosion behavior of a novel high-Zn containing Al-Zn-Mg-Cu alloy, Journal of Materials Engineering and Performance, 34 (2025) 5843–5855.

https://doi.org/10.1007/s11665-024-09593-2

[22] Y. Liu, Z. Zhao, G. Wang, Effect of over-aging degree on microstructures, precipitation kinetics, and mechanical properties of an ultra-high-strength Al-Zn-Mg-Cu alloy, Coatings, 14 (2024) 1415. https://doi.org/10.3390/coatings14111415

[23] Z. Zhang, H. Hou, Y. Zhang, M.E. El Sayed, M.N. Murshed, A. Samir, P. Wu, C. Gong, H. Yong, G. Song, D. Fang, D. Sridhar, H. Algadi, B. Liu, Effect of calcium addition on the microstructure, mechanical properties, and corrosion behavior of AZ61-Nd alloy, Advanced Composites and Hybrid Materials, 6 (2023) 50. https://doi.org/10.1007/s42114-023-00631-6

[24] V. Doroshenko, P. Shurkin, T. Sviridova, A. Fortuna, I. Shkaley, Phase composition and microstructure of cast Al-6%Mg-2%Ca-2%Zn alloy with Fe and Si additions, Metals, 13 (2023) 1584. https://doi.org/10.3390/met13091584

[25] Y. Zou, X. Chen, B. Chen, Effects of Ca concentration on degradation behavior of Zn-x Ca alloys in Hank's solution, Materials Letters, 218 (2018) 193–196. https://doi.org/10.1016/j.matlet.2018.02.018

[26] N.A. Belov, E.A. Naumova, T.K. Akopyan, Effect of calcium on structure, phase composition and hardening of Al-Zn-Mg alloys containing up to 12wt.%Zn, Materials Research, 18 (2015) 1384–1391. https://doi.org/10.1590/1516-1439.036415

[27] D.P. Mondal, N. Jha, A. Badkul, S. Das, M.S. Yadav, P. Jain, Effect of calcium addition on the microstructure and compressive deformation behaviour of 7178 aluminium alloy, Materials & Design, 32 (2011) 2803–2812. https://doi.org/10.1016/j.matdes.2010.12.056

[28] J.H. Liu, C.X. Huang, S.D. Wu, Z.F. Zhang, Tensile deformation and fracture behaviors of high purity polycrystalline zinc, Materials Science and Engineering: A, 490 (2008) 117–125. https://doi.org/10.1016/j.msea.2008.01.004

[29] Z. Liu, D. Qiu, F. Wang, J.A. Taylor, M. Zhang, Effect of grain refinement on tensile properties of cast zinc alloys, Metallurgical and Materials Transactions A, 47 (2016) 830–841.

https://doi.org/10.1007/s11661-015-3229-1

OPTIMIZACIJA DODATAKA KALCIJUMA RADI USPOSTAVLJANJA RAVNOTEŽE IZMEĐU ČVRSTOĆE I OTPORNOSTI NA KOROZIJU U LEGURAMA Zn–Al–Cu–Mg KOJE SU GNJEČENE PRI LIVENJU (SQUEEZE-CASTING)

T. Gopalakrishnan *, S.R. Sankaranarayanan, S.P.K. Babu

Katedra za metalurško i materijalno inženjerstvo, Nacionalni institut za tehnologiju, Tiručirapali, Indija

Apstrakt

U ovom istraživanju ispitivane su legure Zn–Al–Cu–Mg koje su gnječene pri livenju (squeeze-casting) sa različitim dodacima kalcijuma (Ca) (0, 0,5, 1,0 i 1,5 mas.%) radi procene kombinovanog uticaja mikrostrukturne evolucije na mehanička svojstva i otpornost na koroziju. Analiza mikrostrukture pokazala je prelaz sa krupnih dendrita bogatih cinkom u osnovnoj leguri na fino zrno i ujednačenu morfologiju pri dodatku kalcijuma do 1,0 mas.%, dok je pri 1,5 mas.% Ca uočeno grubljenje strukture i povećana poroznost usled formiranja prekomerne količine intermetalnih faza. Ispitivanje mehaničkih svojstava pokazalo je da je legura sa 1,0 mas.% Ca imala najveću tvrdoću (141 HV0.1) i zateznu čvrstoću (359 MPa), što se pripisuje prečišćavanju zrna i ojačavanju disperzijom, iako sa smanjenom duktilnošću usled krtosti intermetalnih jedinjenja. Elektrohemijska ispitivanja korozije u rastvoru NaCl od 3,5 mas.% pokazala su da se brzina korozije smanjila od osnovne legure do one sa 1,0 mas.% Ca, potvrđujući poboljšanu otpornost na koroziju zahvaljujući mikrostrukturnom prečišćavanju i formiranju zaštitnog filma. Međutim, prekomeran dodatak Ca (1,5 mas.%) povećao je brzinu korozije na 0,8109 mpy zbog krupnih intermetalnih jedinjenja i poroznosti, što je promovisalo lokalizovani napad. Rezultati istraživanja ukazuju da optimalan dodatak kalcijuma od 1,0 mas.% obezbeđuje ravnotežu između čvrstoće, tvrdoće i otpornosti na koroziju, čineći Ca-modifikovane legure Zn–Al–Cu–Mg perspektivnim kandidatima za strukturne i funkcionalne primene.

Ključne reči: *Gnječene pri livenju (Squeeze casting); Cink-aluminijumska legura; Mehanička svojstva; Otpornost na koroziju*